

RESEARCH ARTICLE



ISSN: 2321-7758

POWER QUALITY IMPROVEMENT IN ELECTRIFIED TRANSPORTATION BY USING A SINGLE-PHASE ACTIVE DEVICE

G.RAMA KRISHNA¹, D.SWASTIK²

^{1,2}Assistant Professor

Christu Jyothi Institute of Technology & Science
Warangal, Telangana, India.



G.RAMA KRISHNA



D.SWASTIK

ABSTRACT

A transformer less hybrid series active filter is proposed to enhance the power quality in single-phase systems with critical loads. This paper assists the energy management and power quality issues related to electric transportation and focuses on improving electric vehicle load connection to the grid. The control strategy is designed to prevent current harmonic distortions of nonlinear loads to flow into the utility and corrects the power factor of this later. While protecting sensitive loads from voltage disturbances, sags, and swells initiated by the power system, riddled of the series transformer, the configuration is advantageous for an industrial implementation. This poly-valent hybrid topology allowing the harmonic isolation and compensation of voltage distortions could absorb or inject the auxiliary power to the grid. Aside from practical analysis, this paper also investigates on the influence of gains and delays in the real-time controller stability. The simulations and experimental results presented in this paper were carried out on a 2-kVA laboratory prototype demonstrating the effectiveness of the proposed topology.

Key Words—Current harmonics, electric vehicle, hybrid series active filter (HSeAF), power quality, real-time control.

©KY Publications

INTRODUCTION

The forecast of future Smart Grids associated with electric vehicle charging stations has created a serious concern on all aspects of power quality of the power system, while widespread electric vehicle battery charging units [1], [2] have detrimental effects on power distribution system harmonic voltage levels [3]. On the other hand, the growth of harmonics fed from nonlinear loads like electric vehicle propulsion battery chargers [4], [5], which indeed have detrimental impacts on the power system and affect plant equipment, should

be considered in the development of modern grids. Likewise, the increased rms and peak value of the distorted current waveforms increase heating and losses and cause the failure of the electrical equipment. Such phenomenon effectively reduces system efficiency and should have properly been addressed [6], [7].

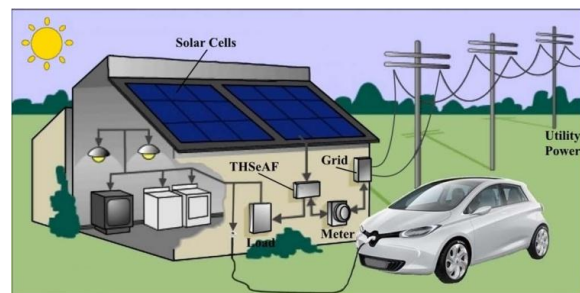
Moreover, to protect the point of common coupling (PCC) from voltage distortions, using a dynamic voltage restorer (DVR) function is advised. A solution is to reduce the pollution of power electronics-based loads directly at their source.

Although several attempts are made for a specific case study, a generic solution is to be explored. There exist two types of active power devices to overcome the described power quality issues. The first category are series active filters (SeAFs), including hybrid-type ones. They were developed to eliminate current harmonics produced by nonlinear load from the power system. SeAFs are less scattered than the shunt type of active filters [8], [9]. The advantage of the SeAF compared to the shunt type is the inferior rating of the compensator versus the load nominal rating [10]. However, the complexity of the configuration and necessity of an isolation series transformer had decelerated their industrial application in the distribution system. The second category was developed in concern of addressing voltage issues on sensitive loads. Commonly known as DVR, they have a similar configuration as the SeAF. These two categories are different from each other in their control principle. This difference relies on the purpose of their application in the system.

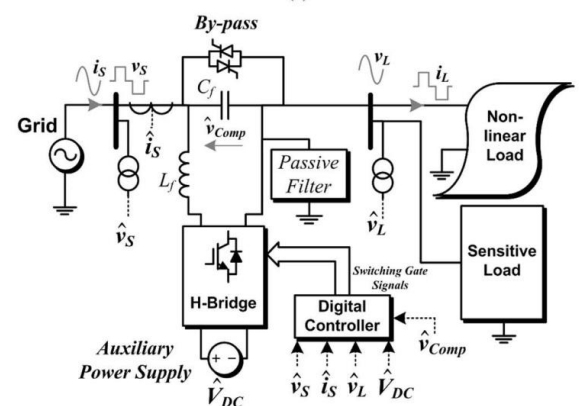
The hybrid series active filter (HSeAF) was proposed to address the aforementioned issues with only one combination. Hypothetically, they are capable to compensate current harmonics, ensuring a power factor (PF) correction and eliminating voltage distortions at the PCC [11], [12]. These properties make it an appropriate candidate for power quality investments. The three-phase SeAFs are well documented [13], [14], whereas limited research works reported the single-phase applications of SeAFs in the literature. In this paper, a single-phase transformerless HSeAF is proposed and capable of cleaning up the grid-side connection bus bar from current harmonics generated by a nonlinear load [15]. With a smaller rating up to 10%, it could easily replace the shunt active filter [16]. Furthermore, it could restore a sinusoidal voltage at the load PCC.

The advantage of the proposed configuration is that non-linear harmonic voltage and current producing loads could be effectively compensated. The transformerless hybrid series active filter (THSeAF) is an alternative option to conventional power transferring converters in

distributed generation systems with high penetration of renewable energy sources, where each phase can be controlled separately and could be operated independently of other phases [17]. This paper shows that the separation of a three-phase converter into single-phase H-bridge converters has allowed the elimination of the costly isolation transformer and promotes industrial application for filtering purposes. The setup has shown great ability to perform requested compensating tasks for the correction of current and voltage distortions, PF correction, and voltage restoration on the load terminal [18].



(a)



(b)

Fig. 1. (a) Schematic of a single-phase smart load with the compensator installation. (b) Electrical diagram of the THSeAF in a single-phase utility. This paper is organized as follows. The system architecture is introduced in the following section. Then, the operation principle of the proposed configuration is explained. The third section is dedicated to the modeling and analysis of the control algorithm implemented in this work. The dc voltage regulation and its considerations are briefly explained, and the voltage and current harmonic detection method is explicitly described. To evaluate

the configuration and the control approach, some scenarios are simulated. Experimental results performed in the laboratory are demonstrated to validate simulations. This paper is summarized with a conclusion and appendix where further mathematical developments are demonstrated.

II. SYSTEM ARCHITECTURE

A. System Configuration

The THSeAF shown in Fig. 1 is composed of an H-bridge converter connected in series between the source and the load. A shunt passive capacitor ensures a low impedance path for current harmonics. A dc auxiliary source could be connected to inject power during voltage sags. The dc-link energy storage system is described in [19]. The system is implemented for a rated power of 2200 VA. To ensure a fast transient response with sufficient stability margins over a wide range of operation, the controller is implemented on a dSPACE/dsp1103. The system parameters are identified in Table I. A variable source of 120 Vrms is connected to a 1.1-kVA nonlinear load and a 998-VA linear load with a 0.46 PF. The THSeAF is connected in series in order to inject the compensating voltage. On the dc side of the compensator, an auxiliary dc-link energy storage system is installed. Similar parameters are also applied for practical implementation.

TABLE I: CONFIGURATION PARAMETERS

Symbol	Definition	Value
v_s	Line phase-to-neutral voltage	120 Vrms
f	System frequency	60 Hz
$R_{non-linear\ load}$	Load resistance	11.5 Ω
$L_{non-linear\ load}$	Load inductance	20 mH
P_L	Linear load power	1 kVA
PF	Linear load power factor	46 %
L_f	Switching ripple filter inductance	5 mH
C_f	Switching ripple filter capacitance	2 μ F
T_S	dSPACE Synchronous sampling time	40 μ s
f_{PWM}	PWM frequency	5 kHz
G	Control gain for current harmonics	8 Ω
V_{DCref}^*	VSI DC bus voltage of the THSeAF	70 V
PI_G	Proportional gain (K_p), Integral gain (K_i)	0.025(4*), 10 (10*)

* Adopted value for the experimental setup

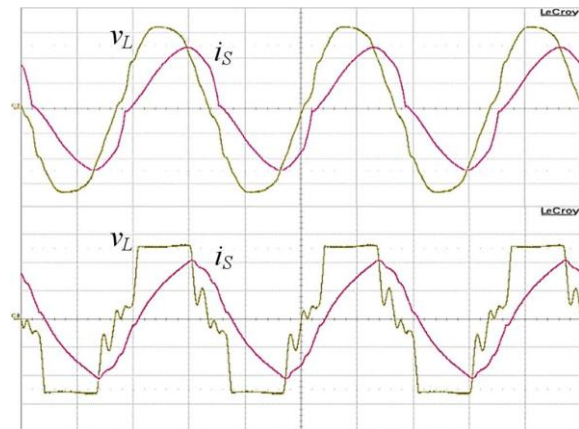


Fig. 2. Terminal voltage and current waveforms of the 2-kVA single-phase system without compensator. (a) Regular operation. (b) Grid's voltage distortion (scales: 50 V/div for channel 1 and 10 A/div for channel 2).

HSeAFs are often used to compensate distortions of the current type of nonlinear loads. For instance, the distorted current and voltage waveforms of the nonlinear system during normal operation and when the source voltage became distorted are depicted in Fig. 2. The THSeAF is bypassed, and current harmonics flowed directly into the grid. As one can perceive, even during normal operation, the current harmonics (with a total harmonic distortion (THD) of 12%) distort the PCC, resulting in a voltage THD of 3.2%. The behavior of the system when the grid is highly polluted with 19.2% of THD is also illustrated. The proposed configuration could be solely connected to the grid with no need of a bulky and costly series injection transformer, making this topology capable of compensating source current harmonics and voltage distortion at the PCC. Even if the number of switches has increased, the transformerless configuration is more cost-effective than any other series compensators, which generally uses a transformer to inject the compensation voltage to the power grid. The optimized passive filter is composed of 5th, 7th, and high-pass filters. The passive filter should be adjusted for the system upon load and government regulations. A comparison between different existing configurations is given in Table II. It is aimed to point out the advantages and disadvantages of the

proposed configuration over the conventional topologies. To emphasize the comparison table fairly, the equivalent single phase of each configuration is considered in the evaluation. Financial production evaluation demonstrated a 45% reduction in component costs and considerable reduction in assembly terms as well.

B. Operation Principle

The SeAF represents a controlled voltage source (VSI). In order to prevent current harmonics i_{Lh} to drift into the source, this series source should present low impedance for the fundamental component and high impedance for all harmonics as shown in Fig. 3. The principle of such modeling is well documented in [20].

The use of a well-tuned passive filter is then mandatory to perform the compensation of current issues and maintaining a constant voltage free of distortions at the load terminals. The behavior of the SeAF for a current control approach is evaluated from the phasor's equivalent circuit shown in Fig. 3. The nonlinear load could be modeled by a resistance representing the active power consumed and a current source generating current harmonics. Accordingly, the impedance Z_L represents the nonlinear load and the inductive load.

The SeAF operates as an ideal controlled voltage source (V_{comp}) having a gain (G) proportional to the current harmonics (I_{sh}) flowing to the grid (V_s)

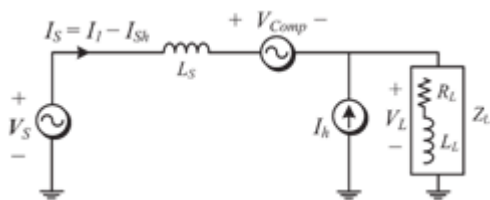


Fig. 3. THSeAF equivalent circuit for current harmonics.

The SeAF operates as an ideal controlled voltage source (V_{comp}) having a gain (G) proportional to the current harmonics (I_{sh}) flowing to the grid (V_s)

$$V_{comp} = G \cdot I_{sh} - V_{Lh} \quad (1)$$

This allows having individual equivalent circuit for the fundamental and harmonics

$$V_{source} = V_{s1} + V_{sh}, \quad V_L = V_{L1} + V_{Lh} \quad (2)$$

The source harmonic current could be evaluated

$$V_{sh} = -Z_s \cdot I_{sh} + V_{comp} + V_{Lh} \quad (3)$$

$$V_{Lh} = Z_L (I_{Lh} - I_{sh}) \quad (4)$$

Combining (3) and (4) leads to (5)

$$I_{sh} = \frac{V_{sh}}{(G - Z_s)} \quad (5)$$

If gain G is sufficiently large ($G \rightarrow \infty$), the source current will become clean of any harmonics ($I_{sh} \rightarrow 0$). This will help improve the voltage distortion at the grid side. In this approach, the THSeAF behaves as high-impedance open circuit for current harmonics, while the shunt high-pass filter tuned at the system frequency creates a low-impedance path for all harmonics and open circuit for the fundamental; it also helps for PF correction.

III. MODELING AND CONTROL OF THE SINGLE-PHASE THSeAF

A. Average and Small-Signal Modeling

Based on the average equivalent circuit of an inverter [23], the small-signal model of the proposed configuration can be obtained as in Fig. 4. Hereafter, d is the duty cycle of the upper switch during a switching period, whereas \bar{v} and \bar{i} denote the average values in a switching period of the voltage and current of the same leg. The mean converter output voltage and current are expressed by (6) and (7) as follows:

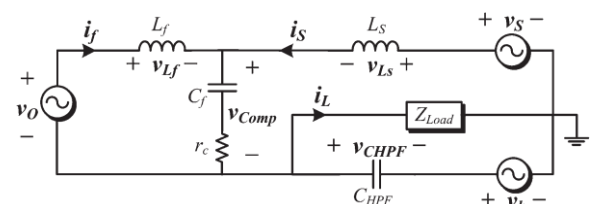


Fig. 4. Small-signal model of transformerless HSeAF in series between the grid and the load.

$$\bar{v}_O = (2d - 1)V_{DC} \quad (6)$$

where the $(2d - 1)$ equals to m , then

$$\bar{i}_{DC} = m \bar{i}_f \quad (7)$$

Calculating the Thevenin equivalent circuit of the harmonic current source leads to the following assumption:

$$\bar{v}_h(j\omega) = \frac{-j \bar{i}_h}{C_{HPF} \cdot \omega_h} \quad (8)$$

If the harmonic frequency is high enough, it is possible to assume that there will be no voltage harmonics across the load. The state-space small-signal ac model could be derived by a linearized perturbation of the averaged model as follows:

$$\dot{x} = Ax + Bu. \quad (9)$$

Hence, we obtain

$$\frac{d}{dt} \begin{bmatrix} \bar{v}_{CF} \\ \bar{v}_{CHPF} \\ \bar{i}_S \\ \bar{i}_f \\ \bar{i}_L \end{bmatrix} = \begin{bmatrix} 0 & 0 & \frac{1}{C_f} & \frac{1}{C_f} & 0 \\ 0 & 0 & \frac{1}{C_{HCPF}} & 0 & -1/C_{HCPF} \\ -1/L_S & -1/L_S & -r_c/L_S & -r_c/L_S & 0 \\ -1/L_f & 0 & -r_c/L_f & -r_c/L_f & 0 \\ 0 & \frac{1}{L_L} & 0 & 0 & -R_L/L_L \end{bmatrix} \times \begin{bmatrix} \bar{v}_{CF} \\ \bar{v}_{CHPF} \\ \bar{i}_S \\ \bar{i}_f \\ \bar{i}_L \end{bmatrix} + \begin{bmatrix} 0 & 0 & 0 \\ 0 & 0 & 0 \\ \frac{1}{L_S} & 0 & \frac{1}{L_S} \\ 0 & \frac{m}{L_f} & 0 \\ 0 & 0 & -1/L_L \end{bmatrix} \times \begin{bmatrix} \bar{v}_S \\ V_{DC} \\ \bar{v}_h \end{bmatrix}. \quad (10)$$

Moreover, the output vector is

$$y = Cx + Du \quad (11)$$

or

$$\begin{bmatrix} \bar{v}_{comp} \\ \bar{v}_L \end{bmatrix} = \begin{bmatrix} 1 & 0 & r_c & r_c & 0 \\ 0 & 1 & 0 & 0 & 0 \end{bmatrix} \times \begin{bmatrix} \bar{v}_{CF} \\ \bar{v}_{CHPF} \\ \bar{i}_S \\ \bar{i}_f \\ \bar{i}_L \end{bmatrix} + \begin{bmatrix} 0 & 0 & 0 \\ 0 & 0 & -1 \end{bmatrix} \times \begin{bmatrix} \bar{v}_S \\ V_{DC} \\ \bar{v}_h \end{bmatrix}. \quad (12)$$

By means of (10) and (12), the state-space representation of the model is obtained as shown in Fig. 4.

The transfer function of the compensating voltage versus the load voltage, $T_{V_CL}(s)$, and the source current, $T_{CI}(s)$, are developed in the Appendix. Meanwhile, to control the active part independently, the derived transfer function should be autonomous from the grid configuration. The transfer function T_{Vm} presents the relation between the output voltages of the converter versus the duty cycle of the first leg converter's upper switch

$$T_V(s) = \frac{V_{comp}}{V_O} = \frac{r_c C_f s + 1}{L_f C_f s^2 + r_c C_f s + 1} \quad (13)$$

$$T_{Vm}(s) = \frac{V_{comp}}{m} = V_{DC} \cdot T_V(s). \quad (14)$$

The further detailed derivation of steady-state transfer functions is described in Section V.

A dc auxiliary source should be employed to maintain an adequate supply on the load terminals. During the sag or swell conditions, it should absorb or inject power to keep the voltage magnitude at the load terminals within a specified margin. However, if the compensation of sags and swells is less imperative, a capacitor could be deployed. Consequently, the dc-link voltage across the capacitor should be regulated as demonstrated in Fig. 5.

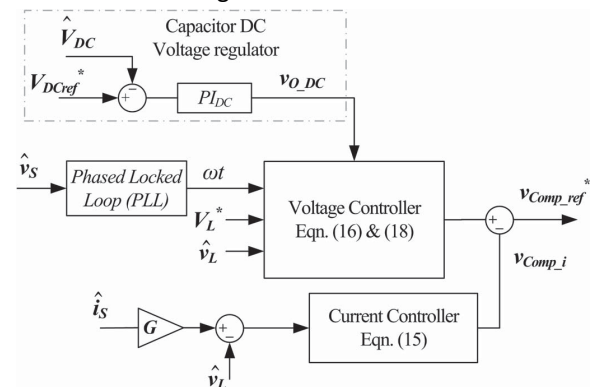


Fig. 5. Control system scheme of the active part.

B. Voltage and Current Harmonic Detection

The outer-loop controller is used where a capacitor replaces the dc auxiliary source. This control strategy is well explained in the previous section. The inner-loop control strategy is based on an indirect control principle. A fast Fourier transformation was used to extract the magnitude of the fundamental and its phase degree from current harmonics. The control gain G representing the impedance of the source for current harmonics has a sufficient level to clean the grid from current harmonics fed through the nonlinear load.

The second proportional integrator (PI) controller used in the outer loop was to enhance the effectiveness of the controller when regulating the dc bus. Thus, a more accurate and faster transient response was achieved without compromising the compensation behavior of the system. According to the theory, the gain G should be kept in a suitable level, preventing the harmonics from flowing into the grid [22], [24]. As previously discussed, for a more precise compensation of current harmonics, the voltage harmonics should also be considered.

The compensating voltage for current harmonic compensation is obtained from

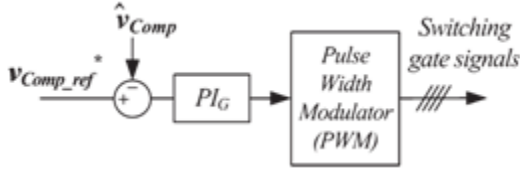


Fig. 6. Block diagram of THSeAF and PI controller

$$v_{comp_i}(t) = (-G\hat{i}_S + \hat{v}_L) - [-Gi_{S1} + v_{L1}] \cdot \sin(\omega st - \theta). \quad (15)$$

Hereby, as voltage distortion at the load terminals is not desired, the voltage sag and swell should also be investigated in the inner loop. The closed-loop equation (16) allows to indirectly maintain the voltage magnitude at the load side equal to V_L^* as a predefined value, within acceptable margins

$$v_{comp_v} = \hat{v}_L - V_L^* \sin(\omega st). \quad (16)$$

The entire control scheme for the THSeAF presented in Fig. 5 was used and implemented in MATLAB/Simulink for real-time simulations and the calculation of the compensating voltage. The real-time toolbox of dSPACE was used for compilation and execution on the dsp-1103 control board. The source and load voltages, together with the source current, are considered as system input signals. According to Srianthumrong et al. [25], an indirect control increases the stability of the system. The source current harmonics are obtained by extracting the fundamental component from the source current

$$v_{com_ref}^* = v_{comp_v} - v_{comp_i} + v_{DC_ref} \quad (17)$$

where the v_{DC_ref} is the voltage required to maintain the dc bus voltage constant

$$v_{DC_ref}(t) = V_{O_DC} \cdot \sin(\omega st). \quad (18)$$

A phase-locked loop was used to obtain the reference angular frequency (ω_s). Accordingly, the extracted current harmonic contains a fundamental component synchronized with the source voltage in order to correct the PF. This current represents the reactive power of the load. The gain G representing the resistance for harmonics converts current into a relative voltage. The generated reference voltage v_{comp_i} required to clean the source current from harmonics is described in (15).

According to the presented detection algorithm, the compen compensated reference voltage $v^*_{Comp_ref}$ is calculated. Thereafter, the reference signal is compared with the measured output voltage and applied to a PI controller to generate the corresponding gate signals as in Fig. 6.

C. Stability Analysis for Voltage and Current Harmonics

The stability of the configuration is mainly affected by the introduced delay of a digital controller. This section studies the impact of the delay first on the inclusive compensated system according to works cited in the literature. Thereafter, its effects on the active compensator is separated from the grid. Using purely inductive source impedance (see Fig. 4) and Kirchhoff's law for harmonic frequency components, (19) is derived. The delay time of the digital controller, large gain G, and the high stiffness of the system seriously affect the stability of the closed-loop controlled system

$$I_{sh}(s) = \frac{V_{sh} - V_{Comp} - V_{Lh}}{L_s s}. \quad (19)$$

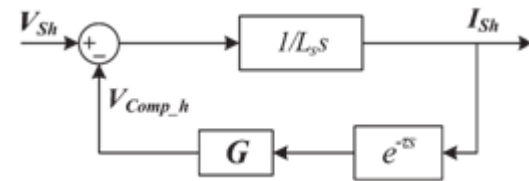


Fig. 7. Control diagram of the system with delay.

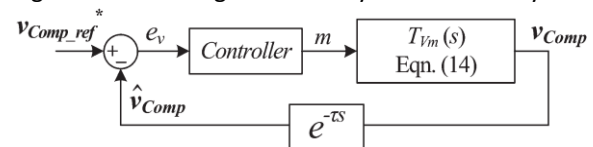


Fig. 8. Closed-loop control diagram of the active filter with a constant delay time τ .

The compensating voltage including the delay time generated by the THSeAF in the Laplace domain [see (1)] is

$$v_{Comp} = G \cdot I_{sh} \cdot e^{-\tau s} - V_{Lh}. \quad (20)$$

Considering (19) and (20), the control diagram of the system with delay is obtained as in Fig. 7.

For the sake of simplicity, the overall delay of the system is assumed to be a constant value τ . Therefore, the open-loop transfer function is obtained

$$G(s) = \frac{G}{L_s s} e^{\tau s}. \quad (21)$$

From the Nyquist stability criterion, the stable operation of the system must satisfy the following condition:

$$G < \frac{\pi L_s}{2\tau}. \quad (22)$$

A system with a typical source inductance L_s of 250 μH and a delay of 40 μs is considered stable according to (22) when the gain G is smaller than 10 Ω . Experimental results confirm the stability of the system presented in this paper. Moreover, the influence of the delay on the control algorithm should also be investigated. According to the transfer functions (13) and (14), the control of the active part is affected by the delay introduced by the digital controller. Thus, assuming an ideal switching characteristic for the IGBTs, the closed-loop system for the active part controller is shown in Fig. 8.

The open-loop transfer function in Fig. 8 turns to (23), where the τ is the delay time initiated by the digital controller

$$F(s) = PI_G \cdot TV_m \cdot e^{\tau s} = \frac{(r_C C_f V_{DC} s + V_{DC}) \cdot (K_p s + K_i) e^{\tau s}}{s \cdot (L_f C_f s^2 + r_C C_f s + 1)}. \quad (23)$$

A PI controller with system parameters described in Table I demonstrates a smooth operation in the stable region. By means of MATLAB, the behavior of the system's transfer function $F(s)$ is traced in Fig. 9. The root locus and the Bode diagram of the compensated open-loop system demonstrate a gain margin of 8.06 dB and a phase margin of 91°. Furthermore, for an extra theoretical investigation, the influence of the delay on the load voltage could also be evaluated with regard to the transfer function $TV_{LS}(s)$ described in the Appendix.

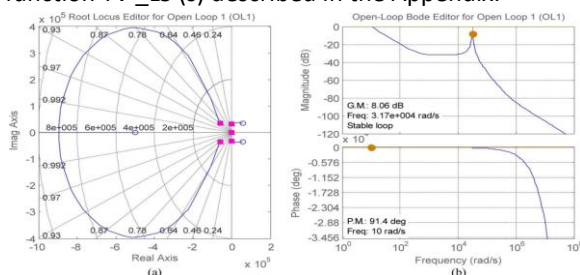


Fig. 9. Compensated open-loop system with delay time of 40 μs . (a) Root locus diagram. (b) Bode diagram.

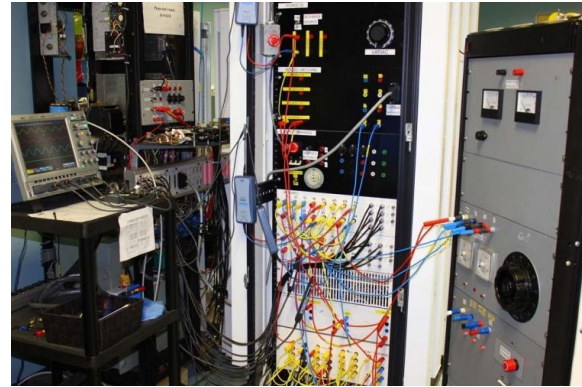


Fig. 10. Transformerless-HSeAF prototype used for experiments

IV. SIMULATIONS AND EXPERIMENTAL RESULTS

The proposed transformerless-HSeAF configuration was simulated in MATLAB/Simulink using discrete time steps of $T_s = 10 \mu\text{s}$. A dSPACE/dsp1103 was used for the fast control prototyping. To ensure an error-free and fast implementation, the complete control loop was executed every 40 μs . The parameters are identified in Table I.

The combination of a single-phase nonlinear load and a linear load with a total rated power of 2 kVA with a 0.74 lagging PF is applied for laboratory experiments and simulations. For experiments and simulations, a 2-kVA 120-Vrms 60-Hz variable source is used. THSeAF connected in series to the system compensates the current harmonics and voltage distortions. The complete experimental system is demonstrated in Fig. 10.

A gain $G = 8 \Omega$ equivalent to 1.9 p.u. was used to control current harmonics. As mentioned earlier, the capability of operation with low dc voltage is considered as one of the main advantages of the proposed configuration. For this experiment, it is maintained at 130 Vdc. During a grid's voltage distortion, the compensator regulates the load voltage magnitude, compensates current harmonics, and corrects the PF. The simulated results of the THSeAF illustrated in Fig. 11 demonstrates improvement in the source current THD. The load

terminal voltage VL THD is 4.3%, while the source voltage is highly distorted (THD VS = 25%).

The grid is cleaned of current harmonics with a unity power factor (UPF) operation, and the THD is reduced to less than 1% in normal operation and less than 4% during grid perturbation. While the series controlled source cleans the current of harmonic components, the source current is forced to be in phase with the source voltage. The series compensator has the ability to slide the load voltage in order for the PF to reach unity. Furthermore, the series compensator could control the power flow between two PCCs.

Experimental results obtained in the laboratory corroborate the successful operation of the THSeAF shown in simulations. Figs. 12 and 13 show the compensator during steady state operating with parameters described in Table I. The source current became sinusoidal, and the load voltage was regulated at rated 120 Vrms. The source current is in phase with the utility voltage, achieving a unity PF correction. The grid supplies 1.545 kVA at a PF equal to 0.99, while the load consumes 2 kVA with a PF of 0.75.

The compensator shows high efficiency in normal operation where the total compensator losses including switching, inductor resistances, and damping resistances are equal to 44 W which is less than 2.5% of the system rated power. The power flow and THD of measured values are depicted in Table III for the case demonstrated in Fig. 12.

The experimented results illustrate a high fidelity with results observed in simulation. Therefore, the system is subjected to sag and swells initiated from the utility source as shown in the following figures. While cleaning the source current from harmonics and correcting the PF, the compensator regulates the load terminal voltage. Clarified in Section III, the auxiliary source provides the necessary amount of power to maintain the supply at the load terminals despite variation in the source magnitude. The behavior of the proposed compensator during dynamic load variation could be depicted from Fig. 14, where the load is suddenly changed.

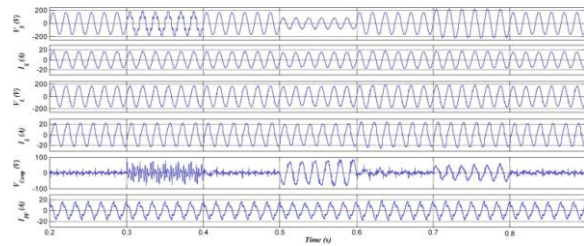


Fig. 11. Simulation of the system with the THSeAF compensating current harmonics and voltage regulation. (a) Source voltage v_S , (b) source current i_S , (c) load voltage v_L , (d) load current i_L , (e) active-filter voltage V_{Comp} , and (f) harmonics current of the passive filter i_{PF} .

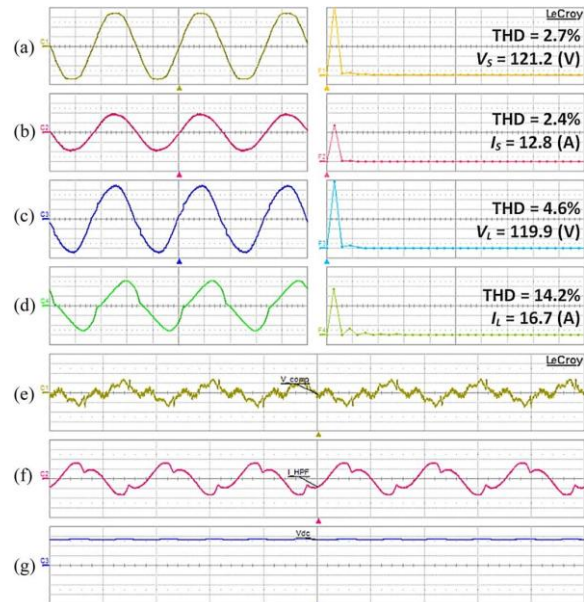


Fig. 12. Experimental waveforms and harmonic spectrum under steady-state sinusoidal grid voltage. (a) Source voltage v_S [50 V/div], (b) source current i_S [10 A/div], (c) load terminal voltage v_L [50 V/div], (d) load current i_L [10 A/div], (e) THSeAF voltage v_{Comp} [20 V/div], (f) passive filter current i_{PF} [10 A/div], and (g) dc voltage v_{DC} [50 V/div].

The THSeAF reacts instantly to this variation and does not interfere its operation functionality. Meanwhile, it is normal to observe a slight transient voltage variation depending on the momentum of the load disengagement or connection.

To evaluate the compensator during utility perturbation, the power source became distorted as depicted in Fig. 15. The source current became cleaned of the majority of harmonics available in the load current and has a unity PF. The THSeAF

prevents existing perturbation on the grid's voltage to propagate on the load PCC. It protects sensitive loads and maintains a sinusoidal and regulated voltage across the PCC of loads with a 3.9% of distortion. Moreover, in a worst possible scenario, the already distorted utility's voltage is subjected to voltage magnitude variation. Thus, the compensator should also inject power to maintain the load PCC voltage regulated at the desired level.

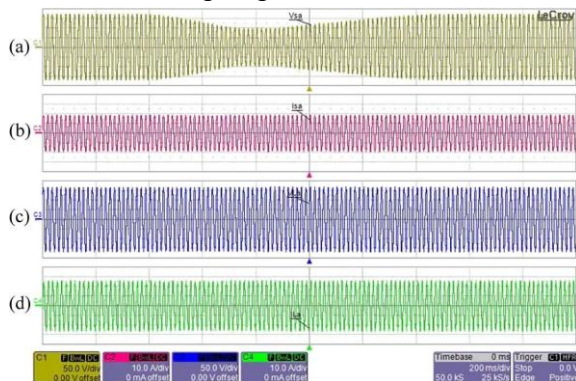


Fig. 13. Waveforms during a variation of the source voltage. (a) Source voltage v_S [50 V/div], (b) source current i_S [10 A/div], (c) load PCC voltage v_L [50 V/div], and (d) load current i_L [10 A/div].

TABLE III: LABORATORY MEASURED VALUE AND POWER FLOW ANALYSIS

Measures	Load		Grid Utility (Source)	
	Voltage (V), V_L	Current (A), I_L	Voltage (V), V_S	Current (A), I_S
THD (%)	4.6	14.2	2.7	2.4
Fund. (rms)	119.9	16.7	121.2	12.8
Active power, P (W)	1499.7		1544.4	
Reactive power, Q (var)	1284.5		10.6	
Power, S (VA)	1998.6		1545.2	
Power Factor, PF	0.75		0.99	
Compensator, THSeAF	$S_{Comp} = +44W - j1274var$			

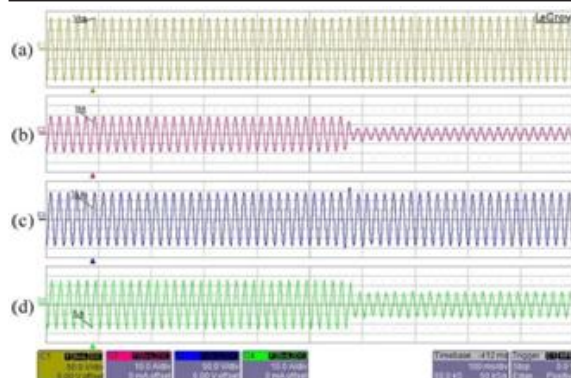


Fig. 14. Waveforms during a dynamic load variation. (a) Source voltage v_S [50 V/div], (b) source current i_S [10 A/div], (c) load PCC voltage v_L [50 V/div], and (d) load current i_L [10 A/div].

i_S [10 A/div], (c) load PCC voltage v_L [50 V/div], and (d) load current i_L [10 A/div].

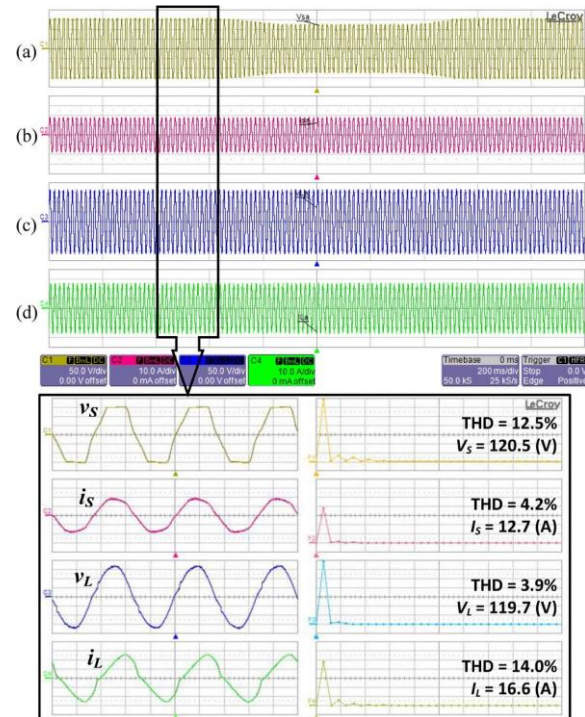


Fig. 15. Experimental waveforms under utility voltage distortion and prolonged sags. (a) Utility source voltage v_S [50 V/div], (b) utility current i_S [10 A/div], (c) load PCC voltage v_L [50 V/div], and (d) load current i_L [10 A/div].

During voltage sag and swell, the auxiliary source supplies the difference of power to maintain the magnitude of the load side voltage regulated. The harmonic content and THD factor of the source utility and load PCC presented show dramatic improvements in THD, while the load draws polluted current waveforms. Furthermore, although the grid's voltage is polluted, the compensator in a hybrid approach regulates and maintains a harmonic-free load voltage.

V. SUMMARY

In this paper, a transformerless HSeAF for power quality improvement was developed and tested. The paper highlighted the fact that, with the ever increase of nonlinear loads and higher exigency of the consumer for a reliable supply, concrete actions should be taken into consideration for future smart grids in order to smoothly integrate electric car battery chargers to the grid. The key novelty of the

proposed solution is that the proposed configuration could improve the power quality of the system in a more general way by compensating a wide range of harmonics current, even though it can be seen that the THSeAF regulates and improves the PCC voltage. Connected to a renewable auxiliary source, the topology is able to counteract actively to the power flow in the system. This essential capability is required to ensure a consistent supply for critical loads. Behaving as high-harmonic impedance, it cleans the power system and ensures a unity PF. The theoretical modeling of the proposed configuration was investigated. The proposed transformerless configuration was simulated and experimentally validated. It was demonstrated that this active compensator responds properly to source voltage variations by providing a constant and distortion-free supply at load terminals. Furthermore, it eliminates source harmonic currents and improves the power quality of the grid without the usual bulky and costly series transformer.

APPENDIX

For the sake of simplicity, the resistance r_c of the switching capacitor filter C_f is neglected, and the inductance L_f has an ideal behavior.

A. Relationship of Load Voltage (V_L) and Grid Voltage (V_S)

$$T_{V_{LS}}(s) = \frac{V_L(s)}{V_S(s)} = \frac{Z_{Load}}{L_S + Z_{out} + Z_{Load}} = \frac{L_f L_L C_f s^3 + L_f R_L C_f s^2 + L_L s + R_L}{A + B + C + D + E + F}$$

$$A = L_f L_L L_S C_f C_{HPPF} s^5$$

$$B = L_f L_S R_L C_f C_{HPPF} s^4$$

$$C = (L_f L_L C_f + L_f L_L C_{HPPF} + L_f L_S C_f + L_L L_S C_{HPPF}) s^3$$

$$D = (L_f R_L C_f + L_f R_L C_{HPPF} + L_S R_L C_{HPPF}) s^2$$

$$E = (L_f + L_L + L_S) s, \quad F = R_L.$$

B. Relation Between Load Voltage (V_L) and Compensating Voltage (V_{Comp})

$$T_{V_{CL}}(s) = \frac{V_{Comp}}{V_L} = \frac{Z_{out}}{Z_{Load}} = \frac{L_f L_L C_{HPPF} s^3 + L_f R_L C_{HPPF} s^2 + L_f s}{L_f L_L C_f s^3 + L_f R_L C_f s^2 + L_L s + R_L}$$

REFERENCES

- [1]. L. Jun-Young and C. Hyung-Jun, "6.6-kW onboard charger design using DCM PFC converter with harmonic modulation technique and two-stage dc/dc converter," IEEE Trans. Ind. Electron., vol. 61, no. 3, pp. 1243–1252, Mar. 2014.
- [2]. R. Seung-Hee, K. Dong-Hee, K. Min-Jung, K. Jong-Soo, and L. Byoung-Kuk, "Adjustable frequency duty-cycle hybrid control strategy for full-bridge series resonant converters in electric vehicle chargers," IEEE Trans. Ind. Electron., vol. 61, no. 10, pp. 5354–5362, Oct. 2014.
- [3]. P. T. Staats, W. M. Grady, A. Arapostathis, and R. S. Thallam, "A statistical analysis of the effect of electric vehicle battery charging on distribution system harmonic voltages," IEEE Trans. Power Del., vol. 13, no. 2, pp. 640–646, Apr. 1998.
- [4]. A. Kuperman, U. Levy, J. Goren, A. Zafransky, and A. Savernin, "Battery charger for electric vehicle traction battery switch station," IEEE Trans. Ind. Electron., vol. 60, no. 12, pp. 5391–5399, Dec. 2013.
- [5]. Z. Amjadi and S. S. Williamson, "Modeling, simulation, control of an advanced Luo converter for plug-in hybrid electric vehicle energy-storage system," IEEE Trans. Veh. Technol., vol. 60, no. 1, pp. 64–75, Jan. 2011.
- [6]. H. Akagi and K. Isozaki, "A hybrid active filter for a three-phase 12-pulse diode rectifier used as the front end of a medium-voltage motor drive," IEEE Trans. Power Del., vol. 27, no. 1, pp. 69–77, Jan. 2012.
- [7]. A. F. Zobaa, "Optimal multiobjective design of hybrid active power filters considering a distorted environment," IEEE Trans. Ind. Electron., vol. 61, no. 1, pp. 107–114, Jan. 2014.
- [8]. D. Sixing, L. Jinjun, and L. Jiliang, "Hybrid cascaded H-bridge converter for harmonic current compensation," IEEE Trans. Power Electron., vol. 28, no. 5, pp. 2170–2179, May 2013.
- [9]. M. S. Hamad, M. I. Masoud, and B. W. Williams, "Medium-voltage 12-pulse converter: Output voltage harmonic compensation using a series

- APF," IEEE Trans. Ind. Electron., vol. 61, no. 1, pp. 43–52, Jan. 2014.
- [10]. J. Liu, S. Dai, Q. Chen, and K. Tao, "Modelling and industrial application of series hybrid active power filter," IET Power Electron., vol. 6, no. 8, pp. 1707–1714, Sep. 2013.
- [11]. [11] A. Javadi, H. Fortin Blanchette, and K. Al-Haddad, "An advanced control algorithm for series hybrid active filter adopting UPQC behavior," in Proc. 38th Annu. IEEE IECON, Montreal, QC, Canada, 2012, pp. 5318–5323.
- [12]. O. S. Senturk and A. M. Hava, "Performance enhancement of the single-phase series active filter by employing the load voltage waveform reconstruction and line current sampling delay reduction methods," IEEE Trans. Power Electron., vol. 26, no. 8, pp. 2210–2220, Aug. 2011.
- [13]. A. Y. Goharrizi, S. H. Hosseini, M. Sabahi, and G. B. Gharehpetian, "Three-phase HFL-DVR with independently controlled phases," IEEE Trans. Power Electron., vol. 27, no. 4, pp. 1706–1718, Apr. 2012.
- [14]. H. Abu-Rub, M. Malinowski, and K. Al-Haddad, Power Electronics for Renewable Energy Systems, Transportation, Industrial Applications. Chichester, U.K.: Wiley InterScience, 2014.
- [15]. [15] S. Rahmani, K. Al-Haddad, and H. Kanaan, "A comparative study of shunt hybrid and shunt active power filters for single-phase applications: Simulation and experimental validation," Math. Comput. Simul., vol. 71, no. 4–6, pp. 345–359, Jun. 19, 2006.
- [16]. W. R. Nogueira Santos et al., "The transformerless single-phase universal active power filter for harmonic and reactive power compensation," IEEE Trans. Power Electron., vol. 29, no. 7, pp. 3563–3572, Jul. 2014.
- [17]. A. Javadi, H. Fortin Blanchette, and K. Al-Haddad, "A novel transformerless hybrid series active filter," in Proc. 38th Annu. IEEE IECON, Montreal, QC, USA, 2012, pp. 5312–5317.
- [18]. H. Liqun, X. Jian, O. Hui, Z. Pengju, and Z. Kai, "High-performance indirect current control scheme for railway traction four-quadrant converters," IEEE Trans. Ind. Electron., vol. 61, no. 12, pp. 6645–6654, Dec. 2014.
- [19]. E. K. K. Sng, S. S. Choi, and D. M. Vilathgamuwa, "Analysis of series compensation and dc-link voltage controls of a transformerless self-charging dynamic voltage restorer," IEEE Trans. Power Del., vol. 19, no. 3, pp. 1511–1518, Jul. 2004.
- [20]. H. Fujita and H. Akagi, "A practical approach to harmonic compensation in power systems-series connection of passive and active filters," IEEE Trans. Ind. Appl., vol. 27, no. 6, pp. 1020–1025, Nov./Dec. 1991.
- [21]. A. Varschavsky, J. Dixon, M. Rotella, and L. Mora, "Cascaded nine-level inverter for hybrid-series active power filter, using industrial controller," IEEE Trans. Ind. Electron., vol. 57, no. 8, pp. 2761–2767, Aug. 2010.
- [22]. X. P. n. Salmero and S. P. n. Litra, "A control strategy for hybrid power filter to compensate four-wires three-phase systems," IEEE Trans. Power Electron., vol. 25, no. 7, pp. 1923–1931, Jul. 2010.
- [23]. B. Singh, A. Chandra, and K. Al-Haddad, Power Quality Problems and Mitigation Techniques. Chichester, U.K.: Wiley, 2015.
- [24]. P. Salmeron and S. P. Litran, "Improvement of the electric power quality using series active and shunt passive filters," IEEE Trans. Power Del., vol. 25, no. 2, pp. 1058–1067, Apr. 2010.
- [25]. S. Srianthumrong, H. Fujita, and H. Akagi, "Stability analysis of a series active filter integrated with a double-series diode rectifier," IEEE Trans. Power Electron., vol. 17, no. 1, pp. 117–124, Jan. 2002.